Tunable Terahertz Perfect Absorber and Polarizer Based on one-Dimensional Anisotropic Graphene Photonic Crystal

Shahab Tavana, Abbas Zarifkar, *Senior Member, IEEE*, and Mehdi Miri

***Abstract*—In this article, a new tunable absorber and polarizer using one-dimensional anisotropic graphene photonic crystal (1D AGPC) is proposed for terahertz applications. The optical properties of the 1D AGPC structure is obtained through the transfer matrix method (TMM) calculations. In our design, a single defect layer is introduced in the 1D AGPC structure to increase its absorption. The absorption coefficient is further modified by optimizing the AGPC parameters such as the number of photonic crystal periods, the defect layer thickness, and the chemical potential of graphene. The modified structure can provide perfect absorption with a narrow bandwidth of 0.05 THz. On the other hand, considering the anisotropic optical properties of graphene, polarization dependence of the absorption coefficient is investigated. This feature of the structure can be employed to realize a tunable terahertz polarizer by adjusting incident angle at $\theta_0 = 80^\circ$. In this way, high tunable polarization extinction ratio of 6.1 dB to 11.63 dB with respectively very narrow bandwidth of 0.031 THz to 0.023 THz are obtained. The maximum insertion losses within the tunable frequency range are as low as 0.023 dB and 0.031 dB. Hence, our design may have potential applications in narrow-band optoelectronic devices at the terahertz frequency range.**

***Index Terms*—Anisotropic, graphene-based photonic crystal, photonic bandgap, terahertz absorber, polarizer.**

I. Introduction

OPTICAL absorbers, which absorb electromagnetic (EM) waves via lossy materials, have attracted attentions due to their potential applications such as detectors [1], sensors [2], solar cells [3], and spectroscopy [4]. These absorbers are classified into two categories: single-channel [5] and multichannel [6]. Single-channel absorbers have many applications and are categorized into broadband [7] and narrow-band [8], according to their spectral width. The operation of absorbers in the terahertz radiation range between 1 THz and 10 THz, known as the terahertz gap, is fascinating due to low energy consumption, high penetrability, and high resolution at these frequencies [9]–[11]. During recent decade, researchers have been working on developing tunable optical absorbers. In between, graphene has remarkable interest due to visible transparency, high surface area, low ohmic loss, adjustable Fermi level, and low absorption loss in the terahertz and far infrared (IR) [12], [13]. One-atom-thick graphene with a 2D honeycomb lattice absorbs 2.3% of light in the mentioned frequency ranges. Moreover, through applying an external gate voltage, the chemical potential of graphene and therefore its electrical conductivity can be altered [14]. Among diverse studies, enhancing the absorption of graphene has become a new area of research and various solutions have been proposed regarding this matter, such as metamaterials [15], nanoparticles [16], localized plasmon excitation [17], hybrid nanocomposites [18], metasurfaces [19], and photonic crystals [20].

Combination of graphene and photonic crystals have been explored to manipulate the optical characteristics, conveniently. Photonic crystals (PCs) are constructed of artificial microstructures with a spatially periodic refractive index. The most striking feature of PCs is photonic bandgaps (PBG) that causes electromagnetic waves be reflected by them. This feature allows us to use PCs in applications like Bragg reflectors. PCs are classified into one, two, and three-dimensional based on the direction of periodicity and among them, one-dimensional photonic crystals (1D PCs) are very interesting because of their simple structure and wide applications [21], [22]. Besides, 1D PCs can be easily fabricated by the chemical vapor deposition (CVD) technique [23]. A novel type of PCs is composed of sequential stacks of alternating graphene and dielectric layers which are well-known as one-dimensional graphene photonic crystals (1D GPCs) and have been utilized in many applications such as isolators [24], biosensors [25], modulators [26], faraday rotators [27], and temperature sensors [28]. On the other hand, anisotropy, which is an interesting feature of graphene, results in remarkable optical properties for GPCs [29]–[31]. The complex band structure of the 1D anisotropic graphene photonic crystal (AGPC) has been obtained in [32] by using the transfer matrix method (TMM).

During recent years, various absorbers have been proposed based on photonic crystals. Lu *et al.* designed an absorber constructed of all-dielectric PCs and a thick metal in which an absorption more than 90% in the visible region has been achieved by using optical Tamm state (OTS) [20]. In [33], the OTS mode has led to a broadband omnidirectional absorber in a heterostructure made up of a Cr layer and a 1D PC containing layered hyperbolic metamaterials. In 2019, Luo and Lai proposed a near-perfect omnidirectional absorber by using the impedance matching property of PCs [34]. By utilizing graphene

Manuscript received May 2, 2022; revised May 22, 2022; accepted May 24, 2022. Date of publication May 26, 2022; date of current version June 3, 2022. *(Corresponding author: Abbas Zarifkar.)*

The authors are with the Department of Communication and Electronics, School of Electrical and Computer Engineering, Shiraz University, Shiraz 71348-51154, Iran (e-mail: shahab.tavana@shirazu.ac.ir; zarifkar@shirazu.ac.ir; miri@shirazu.ac.ir).

Digital Object Identifier 10.1109/JPHOT.2022.3178163

in PC structures, the absorption magnitude of the absorbers can be improved about 50% due to large third-order nonlinearity of graphene as a result of field localization in the graphene layer [35]. Gao *et al.* designed a tunable and multifunctional structure based on 1D AGPC in which a phase-change material, VO_2, placed as a defect layer in the middle of the PC. This structure can be used for variety of applications such as band-pass filtering, perfect absorption, and comb-shaped extraordinary optical transmission in the terahertz range [36]. Maghoul *et al.* proposed a tunable terahertz absorber by using fractal triangle-shaped graphene layers between dielectric substrates. It has potential to adjust the narrowing and widening of the absorption spectrum by changing the Fermi level through applying external DC voltage [37]. Lu *et al.* designed a nonreciprocal absorber which is based on an isotropic epsilon-near-zero (ENZ) slab. This structure is strongly independent from the incident angle which causes an absorption peak of 95% for the incident angles between 60° and 70° [38]. By using a 1D PC nanobeam cavity coupled to a graphene layer, a near-infrared absorber with a high quality factor of 1.28×10^6 has been achieved [39].

In this paper, we present a tunable and multifunctional asymmetric device that operates as a perfect absorber and polarizer in the terahertz frequency range. This asymmetric device is comprised of alternating anisotropic graphene and dielectric materials unlike most previous reports on absorbers, which graphene has been used as a defect layer. In our proposed structure a single defect layer is introduced in the middle of 1D AGPC to break the symmetry of the structure, and boost the absorption of graphene at the resonance frequency. Thus, a prefect narrow-band absorber is achieved after modifying the structure, while it can also be adjusted via chemical potential. Moreover, thanks to the anisotropy of graphene, we have attained a tunable polarizer in the terahertz region. To the best of our knowledge, our polarizer has the lowest bandwidth and insertion loss among the recent narrow-band polarizers in the terahertz range. The 2×2 anisotropic transfer matrix method is exploited to analyze the proposed absorber and polarizer performance. The rest of this paper is organized as follows. Section II describes the structure design and the theoretical model of the optical absorber and polarizer. The third section focuses on the dependence of complex photonic band structures of 1D AGPC on the chemical potential and incident angle, as well as optimizing the structure to reach a perfect absorber and polarizer in the terahertz range. Finally, conclusions are presented in Section IV.

II. Theoretical Model and Formulism

Fig. 1 shows the schematic of the 1D AGPC structure which is used in our absorber. In this structure, the layers are placed in the x-y plane and the electromagnetic waves with the wave vector k_0 and the incident angle θ_0 propagate along the z-direction. The geometrical arrangement of the 1D AGPC structure is $(GA)^N$ where G and A represent the graphene and SiO_2 layers with the thicknesses d_g and d_A and the relative permittivities ε_g and ε_A, respectively, and N is number of the periods. The lattice constant of the 1D AGPC structure is $a = d_g + d_A$. ε_0 and ε_{N+1} are the relative permittivities of the input and output planes of the

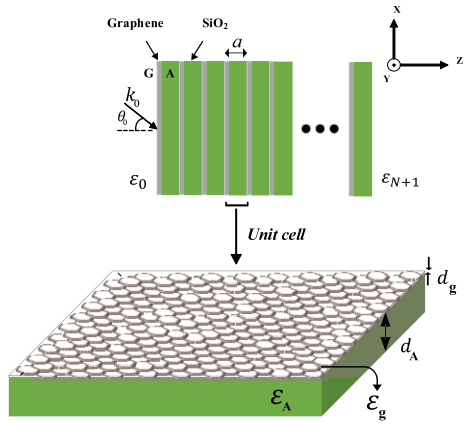

Fig. 1. Schematic of the 1D AGPC stack in which a unit cell consists of a graphene monolayer and a dielectric layer.

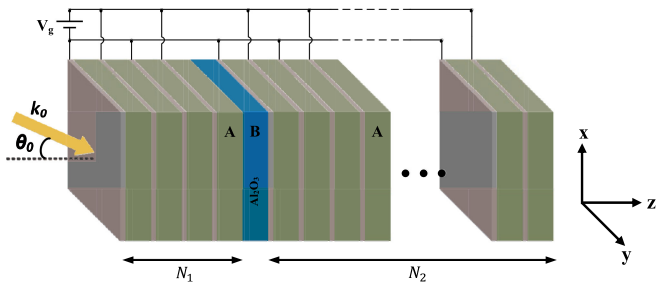

Fig. 2. Sketch of the proposed absorber and polarizer containing a single defect layer. V_g is the applied voltage.

periodic structure which are considered as air mediums. As Fig. 2 depicts, the presented absorber has two 1D AGPC structures with respectively N_1 and N_2 periods at the front and back of the defect layer. The defect layer is an Al_2O_3 dielectric layer with the thickness d_B and relative permittivity ε_B.

There are various methods for simulating the optical properties of 1D AGPC structure, including the plane wave expansion (PWE) [40], green function (GF) [41], finite difference time domain (FDTD) [42], finite element method (FEM) [43], the standard 2×2 transfer matrix method for isotropic layers [29], [44], and 4×4 transfer matrix method that is suitable for all anisotropic layers [45]. Since the thickness of a graphene monolayer is 0.34 nm, simulating the structures containing graphene by using all-numerical methods such as the FEM and FDTD is very time-consuming and requires high simulation facilities. In these situations, a semi-analytical method like the TMM is very useful due to its accurate results and relatively small computational volume.

In order to implement the 2×2 anisotropic TMM, first it is necessary to consider the uniaxial anisotropy of graphene which is because of its 2D nature. The electric permittivity tensor of a graphene stripe in the x-y plane can be given by [32], [46]:

$$\varepsilon_G = \begin{pmatrix} \varepsilon_{G,t} & 0 & 0 \\ 0 & \varepsilon_{G,t} & 0 \\ 0 & 0 & \varepsilon_{G,\perp} \end{pmatrix} \quad (1)$$

The normal component of the graphene permittivity is $\varepsilon_{G,\perp} = 1$, as the normal electric field cannot excite any current in a 2D graphene sheet. The tangential component of the graphene permittivity $\varepsilon_{G,t}$ is expressed as [47]:

$$\varepsilon_{G,t} = 1 + j\frac{\sigma(\omega)}{\varepsilon_0 \omega d_G} \tag{2}$$

where ω is the angular frequency, ε_0 is the permittivity in air and $\sigma(\omega)$ is the surface conductivity of graphene which is calculated according to the Kubo formula as follows [48], [49]:

$$\sigma(\omega) = \sigma_{\text{intra}} + \sigma_{\text{inter}} \tag{3}$$

$$\sigma_{\text{intra}} = -j\frac{e^2 K_B T}{\pi\hbar^2(\omega - j\Gamma)}\left(\frac{\mu_c}{K_B T} + 2\ln\left(e^{-\frac{\mu_c}{K_B T}} + 1\right)\right) \tag{4}$$

$$\sigma_{\text{inter}} = -j\frac{e^2}{4\pi\hbar}\ln\left(\frac{2\mu_c - (\omega - j\Gamma)\hbar}{2\mu_c + (\omega - j\Gamma)\hbar}\right) \tag{5}$$

σ_{intra} and σ_{inter} are the intraband and interband conductivity, respectively. e is the electron charge and μ_c is the chemical potential which obtained as $\mu_c = \hbar v_F\sqrt{\pi n}$, where n is the carrier density and ν_F is the Fermi velocity of electrons. Γ is the scattering rate which is related to the absorption loss, T is the kelvin temperature, $K_B = 1.38\times10^{-23}$ *j/k* is the Boltzmann constant, and $\bar{h}$ is the reduced Planck constant.

As the above equations shows, the surface conductivity of graphene depends on temperature, scattering rate, chemical potential, and frequency. According to the band diagram of graphene, the contribution of the interband electron transitions in conductivity is negligible in the frequency range of less than 10 THz and the surface conductivity is dominated by σ_{intra} [50], [51]. Fig. 3 shows the real and imaginary parts of the tangential permittivity of graphene for different values of chemical potential. As can be seen, in the frequency range of 3 THz to 15 THz, the real part has a negative value while the imaginary part has a positive value. They are strongly influenced by frequency at low frequencies and vary slowly at high frequencies. The behavior of graphene in this range is similar to the behavior of metals such as gold and silver in the visible range. As the chemical potential increases, the real and imaginary parts decrease and increase respectively and shift to higher frequencies.

The incident wave to the structure can be divided into the TE polarization with $\tilde{\text{E}} = (0, \text{E}_\text{y}, 0)$, $\tilde{\text{H}}=(\text{H}_\text{x}, 0, \text{H}_\text{z})$, and the TM polarization with $\tilde{\text{E}}=(\text{E}_\text{x}, 0, \text{E}_\text{z})$, $\tilde{\text{H}}=(0, \text{H}_\text{y}, 0)$. The dispersion relation of the TE polarization for anisotropic graphene is ${k_x}^2 + {k_z}^2 = {k_0}^2\varepsilon_{g,t}$ and for the TM polarization is $\frac{{k_x}^2}{\varepsilon_{g,\perp}} + \frac{{k_z}^2}{\varepsilon_{g,t}} = {k_0}^2$ [48]. when an electromagnetic wave propagates in a 1D AGPC, the electric and magnetic fields at the input and output boundaries of each unit cell can be expressed as follows [32]:

$$\begin{pmatrix} E_x^{out} \\ H_y^{out} \end{pmatrix} = \begin{pmatrix} m_{11} & m_{12} \\ m_{21} & m_{22} \end{pmatrix} \begin{pmatrix} {E_x}^{in} \\ {H_y}^{in} \end{pmatrix} \tag{6}$$

The transfer matrix M_i (i = G, A, and B for graphene, SiO_2 and Al_2O_3, respectively) for each layer can be obtained as:

$$M_i = \begin{pmatrix} \cos(k_{iz}d_i) & -\frac{j}{\eta_i}\sin(k_{iz}d_i) \\ -j\eta_i\sin(k_{iz}d_i) & \cos(k_{iz}d_i) \end{pmatrix} \tag{7}$$

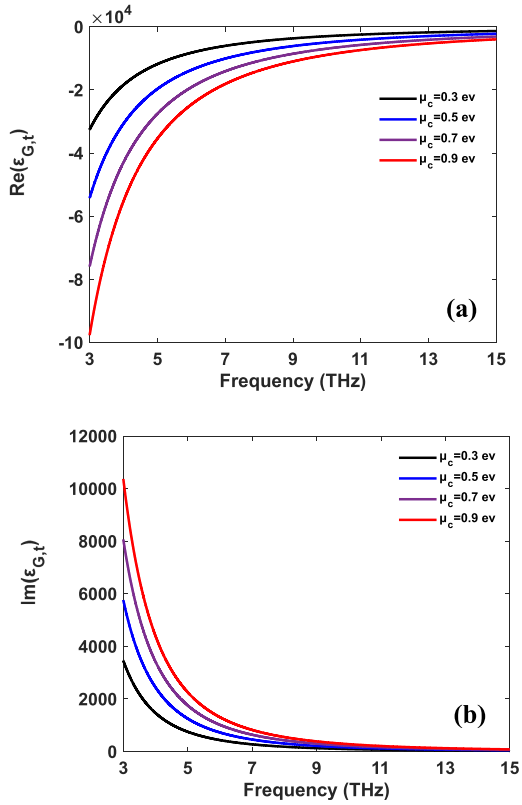

Fig. 3. The (a) Real part and (b) Imaginary part of the tangential permittivity of single-layer graphene versus frequency for different chemical potentials at T = 300 °K.

For the TE polarization, $\eta_i = \frac{k_{iz}}{\omega\mu_0}$ and $k_{iz} = \sqrt{{k_0}^2\varepsilon_i - {k_{ix}}^2}$, where $k_{ix} = k_x = k_0\sin(\theta_0)$. For the TM polarization, $\eta_i = \frac{\omega\varepsilon_0\varepsilon_i}{k_{iz}}$ and $k_{Gz} = \sqrt{{k_0}^2\varepsilon_{G,t} - {k_{ix}}^2(\varepsilon_{G,t}/\varepsilon_{G,\perp})}$, $k_{Az} = \sqrt{{k_0}^2\varepsilon_A - {k_{ix}}^2}$, $k_{Bz} = \sqrt{{k_0}^2\varepsilon_B - {k_{ix}}^2}$ for the graphene, dielectric A and dielectric B layers, respectively. It is clear that whenever the normal incidence is considered, $k_x = 0$ and therefore $k_{Gz} = k_0\sqrt{\varepsilon_{G,t}}$ for both polarizations. Thus, for N periods, the total transfer matrix is:

$$M = (M_G M_A)^N = \begin{pmatrix} m_{11} & m_{12} \\ m_{21} & m_{22} \end{pmatrix} \tag{8}$$

Also, the total transfer matrix for the proposed structure is as follows**:**

$$M = (M_G M_A)^{N_1} M_B (M_G M_A)^{N_2} = \begin{pmatrix} m_{11} & m_{12} \\ m_{21} & m_{22} \end{pmatrix} \tag{9}$$

The reflection coefficient *R,* transmission coefficient *T*, and absorption coefficient *A* can be calculated as follows:

$$\begin{cases} R = |r|^2 \\ T = \begin{cases} |t|^2 (TE) \\ \frac{\eta_0}{\eta_{N+1}}|t|^2 (TM) \end{cases} \\ A = 1 - T - R \end{cases} \tag{10}$$

where

$$t = \left| \left(\frac{2\eta_0}{m_{11}\eta_0 + m_{12}\eta_0\eta_{N+1} + m_{21} + m_{22}\eta_{N+1}} \right) \right|^2 \quad (11)$$

$$r = \left| \left(\frac{m_{11}\eta_0 + m_{12}\eta_0\eta_{N+1} - m_{21} - m_{22}\eta_{N+1}}{m_{11}\eta_0 + m_{12}\eta_0\eta_{N+1} + m_{21} + m_{22}\eta_{N+1}} \right) \right|^2 \quad (12)$$

$$\eta_{N+1} = \begin{cases} \sqrt{\varepsilon_0/\mu_0}\cos(\theta_{N+1}) \\ \sqrt{\varepsilon_0/\mu_0}/\cos(\theta_{N+1}) \end{cases}, \ \eta_0 = \begin{cases} \sqrt{\varepsilon_0/\mu_0}\cos(\theta_0) \\ \sqrt{\varepsilon_0/\mu_0}/\cos(\theta_0) \end{cases} \quad (13)$$

θ_0 and θ_{N+1} are the angles of the input and output wave, respectively.

III. Results and Discussions

In this work, we investigate the optical properties of the 1D AGPC by using the TMM in the frequency range of 0–15 THz. In our calculations, we use SiO_2 as a dielectric material with the relative permittivity of $\varepsilon_A = 2.2$ and thickness of $d_A = 20\ \mu$m. Furthermore, other optical and geometrical parameters of the structure are as follows: $\mu_c = 0.9$ eV, $\Gamma = 1$ THz, $d_g = 0.34$ nm, T = 300 °K and N = 20. Fig. 4(a) represents the real part of the band structure of the 1D AGPC at normal incident angle. The PBGs are the same for both polarizations because the graphene wave vector along the z-axis has the same value ($k_{G,z} = k_0\sqrt{\varepsilon_{G,t}}$). There are three PBGs in the frequency range of 0–15 THz. In the case of $\mu_c = 0.9$ eV, the first gap is located below the cut-off frequency ($f_c = 2.17$ THz). This gap is known as graphene induced photonic band gap (GIPBG), which is created solely due to the presence of graphene monolayer. The more graphene layers are embedded in the structure, the broader PBG is created in the lower frequencies.

The major advantage of this range is tunability of the GIPBG width by controlling the chemical potential. The second gap is from 5.05 THz to 5.9 THz and the third gap is between 10.1 THz to 10.63 THz. These gaps are emerged due to the structural Bragg gap. The appearance of the Bragg PBGs in 1D AGPCs depends on thicknesses, dielectric constants and dispersion properties of the layers. The Fabry-Perot limit at the low edge of the Bragg PBGs for single SiO_2 layer (without graphene sheet) is obtained through $f_p = mc/2d_An_A$, where $m = 12$ is the diffraction order [32]. As shown in Fig. 4(b), the imaginary part has value only in the range of the PBGs, which coincides with the real part of the band structure. The imaginary part indicates the damping coefficient, which is related to the absorption and thermal losses in the bandgap, because the structure in this range is similar to metal-dielectric structures. When the chemical potential of graphene increases from 0.3 eV to 0.9 eV, the lower edges of the GIPBG and the Bragg gaps almost overlap, while the upper edges shift toward the higher-frequency region, and the PBGs enlarge.

Fig. 4(c) and 4(d) depict the transmission and reflection spectra of the 1D AGPC when the chemical potential changes from 0.3 eV to 0.9 eV. It is clear that there are three PBGs regions in which electromagnetic waves are completely reflected, and the oscillations outside the PBG are due to the Fabry-Perot

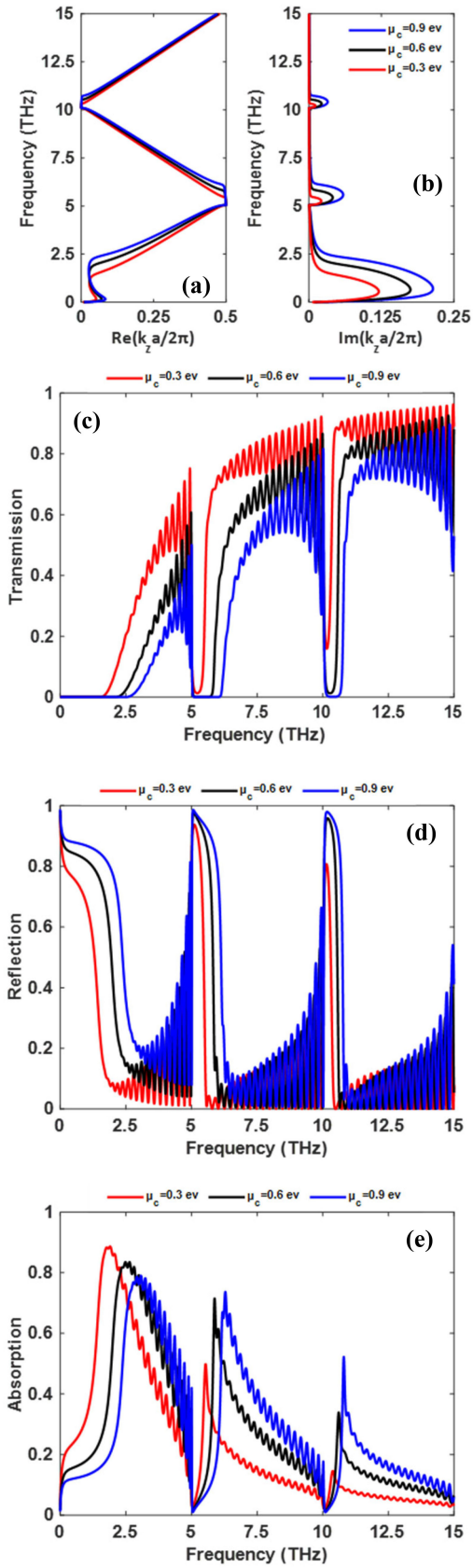

Fig. 4. (a) Real and (b) Imaginary parts of the 1D AGPC band structure for different chemical potentials at normal incidence. (c) Transmission, (d) Reflection, and (e) Absorption spectra of the 1D AGPC.

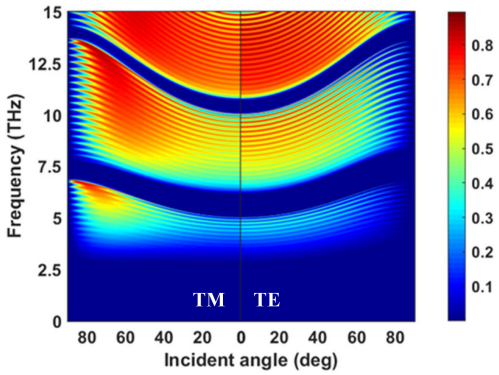

Fig. 5. Color map of the transmission spectra versus the incident angle for the TE and TM polarizations.

oscillations of the Bloch waves at the multilayer boundaries. By increasing the chemical potential of graphene monolayers, the widths of the transmission and reflection peaks become wider and the peaks shift to higher frequencies. On the other hand, increasing the chemical potential leads to rise of the discrepancy of the refractive index of graphene and SiO_2 and it will broaden the PBGs of the 1D AGPC. Fig. 4(e) plots the absorption spectrum at different chemical potentials. The absorption intensity in the PBGs is very low in contrast to its value at the right edge of the PBGs, because the electromagnetic waves at frequencies above the stop bands are absorbed by graphene due to negative dielectric constant. In fact, more wave energy is stored at the surface of graphene and cannot penetrate to the graphene layer due to small thickness and low skin depth [52]. However, the imaginary part of the graphene dielectric constant is much bigger at low frequencies so that the absorption at the right edge of the GIPBG is higher than Bragg PBGs.

Now, we further examine the effect of the incident angle on 1D AGPC when $\mu_c = 0.9$ eV. Fig. 5 shows the color map of the transmission for both the TE and TM polarizations where the incident angle changes from 0° to 90°. It is clear that the GIPBG is insensitive to the incident angle for the TM polarization, whereas the right edge of the metallic PBG shifts slightly to higher frequencies for the TE polarization. This region is strictly omnidirectional for the TM polarization and is suitable for the designing of terahertz filters. However, the Bragg gaps are highly sensitive to the incident angle in a way that the PBGs shift to higher frequencies, and due to the Brewster angle, the width of the forbidden bands starts to shrink for the TM polarization, whereas it becomes broader for the TE polarization.

Based on the above discussions, we present our absorber and polarizer in two following sections, respectively.

A. *The Absorber*

Here, according to Fig. 4, we consider the increment of the absorption in the first Bragg PBG due to high absorption of graphene in the frequency region lower than 6 THz. This is because that in these frequencies, the imaginary part of $\varepsilon_{G,t}$ increases sharply. As shown in Fig. 2, we introduce a single defect layer with the thickness of $d_B = 26\ \mu$m and relative permittivity of $\varepsilon_B = 3.1$ in the middle of the 1D AGPC. When the defect layer is placed between $N_1 = 4$ and $N_2 = 20$ periods, the crystal order is disrupted and turn into an asymmetric structure. The photonic crystals with $N_2 = 20$ reflect the light completely in the PBG. So, the incident wave at the resonance wavelength is trapped in the defect region and it acts as a Fabry-Perot cavity resonator. In fact, the multilayer AGPC on both sides of the defect behave like mirrors and strengthens the interaction between graphene and incident light. As a result, the defect mode is excited and a strong localized field is created in the defect region, which improves the absorption of graphene. Since this absorption depends on the optical and geometrical parameters such as the number of periods, the defect layer thickness, and the chemical potential of graphene, a terahertz perfect absorber can be designed. In the first case, we desire to investigate the effect of the number of periods in the front of the defect layer on the absorption diagram. Fig. 6(a) shows that the absorption spectrum is highly dependent on N_1. By increasing N_1, the absorption peak increases and the bandwidth of the absorption peak decreases. The absorber reaches to the highest absorption for $N_1 = 4$ and the frequency of the defect mode shifts to higher frequencies. When the number of periods rises upper than 4 periods, the absorption peak starts to reduce, because the crystal layers start to reflect the light so that the resonance condition for the light that trapped in the defect region is incomplete and it leaves the crystal. In the second case, we are looking to investigate the effect of the defect layer thickness on the absorption spectrum. As shown in Fig. 6(b), by increasing the thickness of the defect layer, the absorption peak increases and moves toward lower frequencies. In other words, the path that light should travel back and forth in the defect region increases, which leads to increase in the amplitude of the absorption peak. Also, the bandwidth of the absorption peak becomes narrower. Next, we investigate the effect of the chemical potential on the absorption peak. The dependence of the graphene refractive index on its chemical potential could explain the tunability of the absorption spectrum. It is clear that by increasing the chemical potential, the absolute value of $\varepsilon_{G,t}$ increases which leads to augmentation of the graphene refractive index. Moreover, when the chemical potential increases, the imaginary part of the graphene permittivity rises and this could increase the absorption. Fig. 6(c) reveals that by increasing the chemical potential, the absorption gradually increases and reaches to the maximum value for $\mu_c = 0.9$ eV. It is clear that the absorption peak shifts to higher frequencies while the width of the absorption peak moderately decreases. As the chemical potential of graphene rises from 0.3 eV to 0.9 eV with a step of 0.3 eV, the frequency of the defect mode stands at 5.12 THz, 5.24 THz, 5.33 THz and the magnitude reaches to 47%, 83.76%, and 100%, respectively.

Therefore, our absorber with tunability of 0.35 THz/eV has potential application in tunable THz narrow-band filters. Fig. 6(d) shows the reflection, transmission, and absorption spectra of the proposed perfect absorber. Last but not least, the whole thickness of the proposed design is approximately 506 μm.

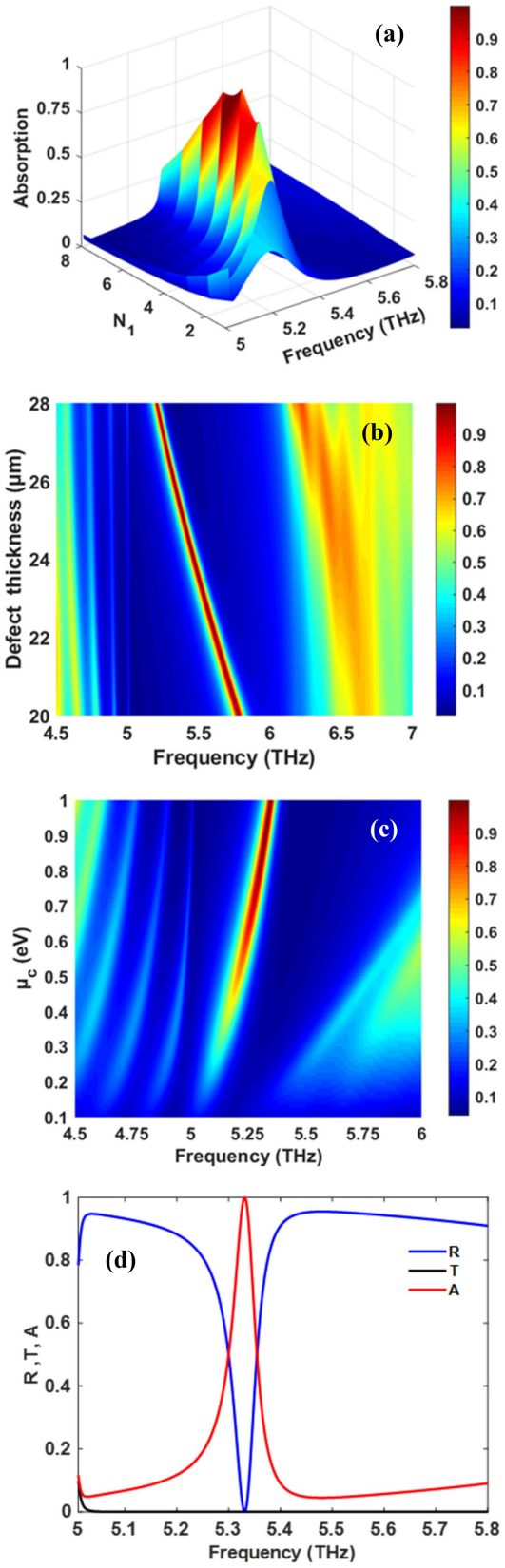

Fig. 6. Color map of the absorption spectrum for (a) Different period numbers N_1, (b) different defect layer thicknesses, and (c) Different chemical potentials. (d) Reflection (R), transmission (T) and absorption (A) spectra of the proposed perfect absorber.

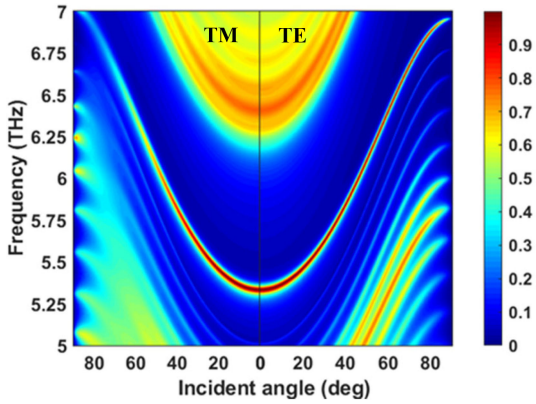

Fig. 7. Color map of the absorption spectrum of the proposed perfect absorber for the TE and TM polarizations as a function of the incident angle.

As can be seen, the defect mode appears at 5.33 THz and the incident light is completely confined in the defect layer that causes an absorption peak of 100%. One of the most important features of the absorber is the bandwidth that can be tuned by changing the chemical potential of graphene. For our proposed structure, the small bandwidth of the absorption peak is equal to 0.05 THz and the absorber has a high-quality factor of 106. Here, the quality factor is calculated by $Q = f_i/\Delta f$, where f_i is the central frequency and Δf is the full-width at half maximum bandwidth. Table I compares the performance of our proposed perfect absorber with the previously reported optical absorbers. It is clear that this perfect absorber has the lowest bandwidth in the terahertz range compared to the previous works.

B. The Polarizer

In this section, we would like to design a terahertz polarizer by using the presented absorber structure. For this, it is necessary to investigate the effect of incident angle on the perfect absorber characteristics. In Fig. 7 the color map of the absorption spectrum is demonstrated for variation of the incident angle from 0° to 90° and for both the TE and TM polarizations. As can be seen, by increasing the incident angle, the absorption peak shifts to higher frequencies for both polarizations with a major difference in terms of magnitude. This displacement is due to the shift of the Bragg PBG of the structure. It is noteworthy that the TM mode is more sensitive to the incident angle than the TE mode. When the incident angle becomes greater than $\theta_0 = 0°$, the absorption intensity for the TM polarization gradually decreases, whereas it remains constant for the TE polarization. The reason is that the graphene wave vector along the z-direction is no longer the same for the TE and TM polarizations [given by (7)]. So, the incident plane waves cannot couple properly to the 1D AGPC for the TM polarization and reflect from the structure, while the coupling is done well for the TE polarization. In fact, the TE waves transmit through the structure and almost completely absorbed.

According to Fig. 8, when light is emitted at $\theta_0 = 80°$, the absorption intensity becomes 0.22 and 0.92 for the TM and TE polarizations, respectively. This feature is suitable for designing a polarizer in the terahertz region. Consequently, the angle of

TABLE I
COMPARISON OF THE PERFORMANCE OF VARIOUS TERAHERTZ ABSORBERS

Structure type	Parameters					
	Center Frequency (THz)	Peak value	Optical Bandwidth (THz)	μ_C(eV)	Tunability (THz/eV)	Total thickness (μm)
graphene-dielectric stacks [53]	0.69-0.92	57%<A<95%	0.14-0.21	0.1-0.5	~0.57	81.2
Thin-film metamaterial [54]	1.72-2.61	45%<A<100%	2.89-3.33	0.1-0.5	~2.22	35.9
graphene-VO_2 metamaterial [55]	1.27-1.35	26%<A<99%	0.71-1.22	0.01-0.5	~0.11	28.7
1D PC with graphene-VO_2 [36]	8.59-8.65	90%<A<100%	0.06-0.08	0.4-1.0	~0.1	550
periodic gold-disks on graphene [56]	9.15-9.41	77.2%<A<96.9%	NA	0.1-0.3	~1.3	1.1
This work	5.12-5.33	47%<A<100%	0.05-0.12	0.3-0.9	~0.35	506

TABLE II
COMPARISON OF THE PERFORMANCE OF VARIOUS TERAHERTZ POLARIZERS

Structure type	Parameters				
	Operating Frequency (THz)	Optical Bandwidth (THz)	ER(dB)	Insertion loss (dB)	μ_C(eV)
Wire grid graphene metal hybrid metasurfaces [57]	0.2-2.5	3	Up to 30	2.54	0.4
Broadband graphene polarizer [58]	193.5	NA	27	5	NA
Graphene/glass hybrid waveguide [59]	219	NA	28	9	0.15-0.35
Textured Graphene gratings [60]	0.001-4	0.65	10-22	2.22	1
Transparent Conducting Oxide [61]	0.1-2.5	2.5	20	2	NA
Double stage graphene nanoribbon [62]	1-4	0.17	Up to 30	0.83-1.87	0.4-0.9
This work	6-7	0.023-0.031	6.1-11.63	0.36-1.3	0.3-0.9

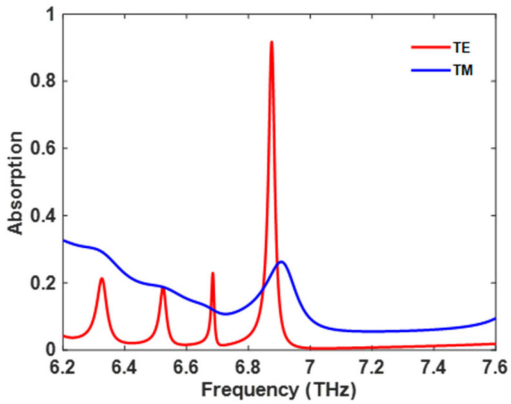

Fig. 8. Absorption curve of the perfect absorber at the incident angle of $\theta_0 = 80°$ for both the TE and TM polarizations.

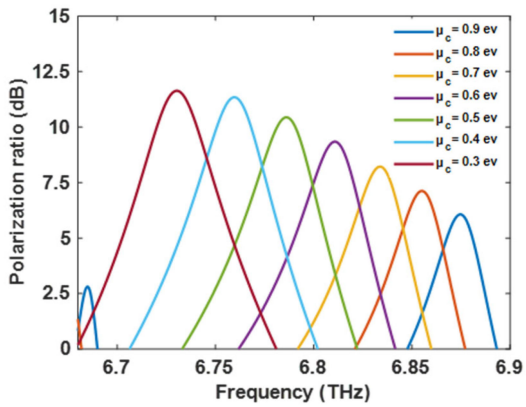

Fig. 9. Calculated polarization extinction ratio of the polarizer as a function of frequency for different chemical potential values.

incidence must be set at $\theta_0 = 80°$ to achieve the terahertz polarizer. the performance of a polarizer can be evaluated by the polarization extinction ratio (PER) which is defined as 10log (A_{TE}/A_{TM}), where A_{TE} and A_{TM} are the absorption of the TE and TM polarization, respectively. The calculated PER for our proposed structure is about 6.1 dB at 6.87 THz at $\theta_0 = 80°$ and $\mu_c = 0.9$ eV. By adjusting the chemical potential of graphene via an external voltage source, the PER can be controlled. Fig. 9 denotes that when the chemical potential of graphene changes from 0.3 eV to 0.9 eV the maximum PER varies from 11.63 dB to and 6.1 dB, respectively. Fig. 9 also shows that the polarizer can be tuned in the range of 6.73 THz to 6.87 THz. It can be concluded that as chemical potential decreases from 0.9 eV to 0.3 eV, the attenuation for the TM mode becomes larger than that of the TE mode. Another important characteristic of polarizer is insertion loss which is given by $-10\log(A_{TE})$.

For the chemical potential of 0.3 eV to 0.9 eV, the insertion loss for the proposed polarizer is calculated as low as 1.3 dB to 0.36 dB, respectively. The optical bandwidth of the polarizer is as low as 0.023 THz and 0.031 THz for $\mu_c = 0.3$ eV and

$\mu_c = 0.9$ eV, respectively. Table II demonstrates the comparison of the presented polarizer with the previously reported polarizers. It shows that our polarizer operates in an important frequency range and not only has the lowest bandwidth among the recent polarizers but also has the lowest insertion loss ever reported for a free-space polarizer.

IV. Conclusion

In summary, we have examined the optical properties of the 1D AGPC in terahertz frequency range by using the TMM. Thanks to a defect layer within the 1D AGPC, a Fabry-Perot cavity is created to enhance the absorption of graphene in the Bragg PBG. Considering variation of different parameters such as the number of periods, the thickness of the defect layer, and the chemical potential of graphene, a perfect absorber in the terahertz range is proposed. Due to high confinement in the defect region, a narrow-band absorber with a bandwidth as low as 0.05 THz is obtained. Finally, we have demonstrated that the absorption of the TE and TM polarizations are dependent on the incident angle because of the anisotropy of graphene, which leads to achieve a tunable terahertz polarizer. According to the calculations, a low bandwidth of 0.023–0.031 THz and a polarization extinction ratio as high as 6.1–11.63 dB are obtained. The presented structure has potential applications in tunable narrow-band filters in THz regions.

References

[1] Y. Zhang, J. Lv, L. Que, G. Mi, Y. Zhou, and Y. Jiang, "A visible-infrared double band photodetector absorber," *Results Phys.*, vol. 18, 2020, Art. no. 103283.

[2] M. Askari, "A near infrared plasmonic perfect absorber as a sensor for hemoglobin concentration detection," *Opt. Quantum Electron.*, vol. 53, no. 2, pp. 1–14, 2021.

[3] F. Ahmad, A. Lakhtakia, and P. B. Monk, "Double-absorber thin-film solar cell with 34% efficiency," *Appl. Phys. Lett.*, vol. 117, no. 3, 2020, Art. no. 033901.

[4] M. Suzuki, O. Boyraz, H. Asghari, and B. Jalali, "Spectral dynamics on saturable absorber in mode-locking with time stretch spectroscopy," *Sci. Rep.*, vol. 10, no. 1, pp. 1–7, 2020.

[5] Y. Jin and K. Yu, "Broadband single-channel coherent perfect absorption with a perfect magnetic mirror," *Opt. Exp.*, vol. 28, no. 23, pp. 35108–35117, 2020.

[6] J. Han, J. Jiang, T. Wu, Y. Gao, and Y. Gao, "Multi-channel high-performance absorber based on SiC-Photonic crystal heterostructure-SiC structure," *Nanomaterials*, vol. 12, no. 2, 2022, Art. no. 289.

[7] T. Xie *et al.*, "High absorption and a tunable broadband absorption based on the fractal technology of infrared metamaterial broadband absorber," *Diamond Related Mater.*, vol. 123, 2022, Art. no. 108872.

[8] M. Pan *et al.*, "A narrowband perfect absorber with high Q-factor and its application in sensing in the visible region," *Results Phys.*, vol. 19, 2020, Art. no. 103415.

[9] M. Wang and E.-H. Yang, "THz applications of 2D materials: Graphene and beyond," *Nano-Struct. Nano-Objects*, vol. 15, pp. 107–113, 2018.

[10] M. Tonouchi, "Cutting-edge terahertz technology," *Nature Photon.*, vol. 1, no. 2, pp. 97–105, 2007.

[11] A. Borak, "Toward bridging the terahertz gap with silicon-based lasers," *Science*, vol. 308, no. 5722, pp. 638–639, 2005.

[12] K. S. Novoselov *et al.*, "Electric field effect in atomically thin carbon films," *science*, vol. 306, no. 5696, pp. 666–669, 2004.

[13] A. G. D'Aloia, M. D'Amore, and M. S. Sarto, "Low-terahertz transparent graphene-based absorber," *Nanomaterials*, vol. 10, no. 5, 2020, Art. no. 843.

[14] Z. Zhen and H. Zhu, "Structure and properties of graphene," in *Graphene*. Amsterdam, The Netherlands: Elsevier, 2018, pp. 1–12.

[15] P. Yu *et al.*, "Broadband metamaterial absorbers," *Adv. Opt. Mater.*, vol. 7, no. 3, 2019, Art. no. 1800995.

[16] L. Escoubas *et al.*, "Design and realization of light absorbers using plasmonic nanoparticles," *Prog. Quantum Electron.*, vol. 63, pp. 1–22, 2019.

[17] Q. Li *et al.*, "Tunable plasmonic absorber based on propagating and localized surface plasmons using metal-dielectric-metal structure," *Plasmonics*, vol. 12, no. 4, pp. 1037–1043, 2017.

[18] V. K. Chakradhary, H. B. Baskey, R. Roshan, A. Pathik, and M. J. Akhtar, "Design of frequency selective surface-based hybrid nanocomposite absorber for stealth applications," *IEEE Trans. Microw. Theory Techn.*, vol. 66, no. 11, pp. 4737–4744, Nov. 2018.

[19] Z. Li, B. Li, Q. Zhao, and J. Zhou, "A metasurface absorber based on the slow-wave effect," *AIP Adv.*, vol. 10, no. 4, 2020, Art. no. 045311.

[20] G. Lu *et al.*, "Perfect optical absorbers by all-dielectric photonic crystal/metal heterostructures due to optical Tamm state," *Nanomaterials*, vol. 11, no. 12, 2021, Art. no. 3447.

[21] E. Yablonovitch, "Inhibited spontaneous emission in solid-state physics and electronics," *Phys. Rev. Lett.*, vol. 58, no. 20, 1987, Art. no. 2059.

[22] L. Han, "1D Photonic crystals: Principles and applications in silicon photonics," in *Theoretical Foundations and Application of Photonic Crystals*. Londan, U.K.: IntechOpen, 2017.

[23] H. Shen, Z. Wang, Y. Wu, and B. Yang, "One-dimensional photonic crystals: Fabrication, responsiveness and emerging applications in 3D construction," *RSC Adv.*, vol. 6, no. 6, pp. 4505–4520, 2016.

[24] M. Zarei, F. Nazari, and M. K. Moravvej-Farshi, "Tunable optical isolator using Graphene-photonic crystal-based hybrid system," *Physica Scripta*, vol. 96, no. 9, 2021, Art. no. 095502.

[25] A. Panda, P. D. Pukhrambam, F. Wu, and W. Belhadj, "Graphene-based 1D defective photonic crystal biosensor for real-time detection of cancer cells," *Eur. Phys. J. Plus*, vol. 136, no. 8, pp. 1–19, 2021.

[26] B. Yu *et al.*, "Magneto-optical and thermo-optical modulations of Goos-Hänchen effect in one-dimensional photonic crystal with graphene-VO_2," *J. Magnetism Magn. Mater.*, vol. 530, 2021, Art. no. 167946.

[27] Y. Liang, Y. Xiang, and X. Dai, "Enhancement of graphene Faraday rotation in the one-dimensional topological photonic crystals," *Opt. Exp.*, vol. 28, no. 17, pp. 24560–24567, 2020.

[28] Z. A. Zaky, A. M. Ahmed, and A. Aly, "Remote temperature sensor based on Tamm resonance," *Silicon*, vol. 14, no. 6, pp. 2765–2777, 2022.

[29] T. Zhan, X. Shi, Y. Dai, X. Liu, and J. Zi, "Transfer matrix method for optics in graphene layers," *J. Phys.: Condens. Matter*, vol. 25, no. 21, 2013, Art. no. 215301.

[30] Y. V. Bludov, N. M. Peres, and M. I. Vasilevskiy, "Unusual reflection of electromagnetic radiation from a stack of graphene layers at oblique incidence," *J. Opt.*, vol. 15, no. 11, 2013, Art. no. 114004.

[31] I. Nefedov and L. Melnikov, "Plasmonic terahertz amplification in graphene-based asymmetric hyperbolic metamaterial," *Photonics*, vol. 2, no. 2 , pp. 594–603, 2015.

[32] L. Qi and C. Liu, "Complex band structures of 1D anisotropic graphene photonic crystal," *Photon. Res.*, vol. 5, no. 6, pp. 543–551, 2017.

[33] F. Wu, X. Wu, S. Xiao, G. Liu, and H. Li, "Broadband wide-angle multilayer absorber based on a broadband omnidirectional optical Tamm state," *Opt. Exp.*, vol. 29, no. 15, pp. 23976–23987, 2021.

[34] J. Luo and Y. Lai, "Near-perfect absorption by photonic crystals with a broadband and omnidirectional impedance-matching property," *Opt. Exp.*, vol. 27, no. 11, pp. 15800–15811, 2019.

[35] H. Wang, F. Ouyang, and Y. Lei, "Enhanced absorption study of one-way absorber based on magnetophotonic crystal combined with graphene," *J. Opt.*, vol. 50, no. 1, pp. 132–141, 2021.

[36] X. Gao, Z. Zhu, J. Yuan, and L. Jiang, "Tunable and multifunctional terahertz devices based on one-dimensional anisotropic photonic crystals containing graphene and phase-change material," *Opt. Exp.*, vol. 29, no. 9, pp. 13314–13330, 2021.

[37] A. Maghoul, A. Rostami, N. Gnanakulasekaran, and I. Balasingham, "Design and simulation of terahertz perfect absorber with tunable absorption characteristic using fractal-shaped graphene layers," *Photonics*, vol. 8, no. 9, 2021, Art. no. 375.

[38] H. Lu *et al.*, "Nonreciprocal Tamm plasmon absorber based on lossy epsilon-near-zero materials," *Opt. Exp.*, vol. 29, no. 12, pp. 17736–17745, 2021.

[39] M. Ferdosian Tehrani, R. Ghayour, and M. Mohitpour, "High-Q and high-absorption photonic crystal nanobeam cavity based on semi-cylinders of air coupled with graphene," *Appl. Phys. A*, vol. 128, no. 1, pp. 1–8, 2022.

[40] J. Bin, Z. Wen-Jun, C. Wei, L. An-Jin, and Z. Wan-Hua, "Improved plane-wave expansion method for band structure calculation of metal photonic crystal," *Chin. Phys. Lett.*, vol. 28, no. 3, 2011, Art. no. 034209.
[41] N. Ouchani, A. El Moussaouy, H. Aynaou, Y. El Hassouani, and B. Djafari-Rouhani, "Optical transmission properties of an anisotropic defect cavity in one-dimensional photonic crystal," *Phys. Lett. A*, vol. 382, no. 4, pp. 231–240, 2018.
[42] Y.-J. Gao, H.-W. Yang, and G.-B. Wang, "A research on the electromagnetic properties of plasma photonic crystal based on the symplectic finite-difference time-domain method," *Optik*, vol. 127, no. 4, pp. 1838–1841, 2016.
[43] H.-M. Lee and J.-C. Wu, "Transmittance spectra in one-dimensional superconductor-dielectric photonic crystal," *J. Appl. Phys.*, vol. 107, no. 9, 2010, Art. no. 09E149.
[44] F. Al-Sheqefi and W. Belhadj, "Photonic band gap characteristics of one-dimensional graphene-dielectric periodic structures," *Superlattices Microstructures*, vol. 88, pp. 127–138, 2015.
[45] J. Hao and L. Zhou, "Electromagnetic wave scatterings by anisotropic metamaterials: Generalized 4×4 transfer-matrix method," *Phys. Rev. B*, vol. 77, no. 9, 2008, Art. no. 094201.
[46] A. Al Sayem, M. M. Rahman, M. Mahdy, I. Jahangir, and M. S. Rahman, "Negative refraction with superior transmission in graphene-hexagonal boron nitride (hBN) multilayer hyper crystal," *Sci. Rep.*, vol. 6, 2016, Art. no. 25442.
[47] D. Guo-Wen *et al.*, "Tunable electromagnetically induced transparency at terahertz frequencies in coupled graphene metamaterial," *Chin. Phys. B*, vol. 24, no. 11, 2015, Art. no. 118103.
[48] Y. Li, L. Qi, J. Yu, Z. Chen, Y. Yao, and X. Liu, "One-dimensional multiband terahertz graphene photonic crystal filters," *Opt. Mater. Exp.*, vol. 7, no. 4, pp. 1228–1239, 2017.
[49] S. Tavana, S. Bahadori-Haghighi, and M. H. Sheikhi, "High-performance electro-optical switch using an anisotropic graphene-based one-dimensional photonic crystal," *Opt. Exp.*, vol. 30, no. 6, pp. 9269–9283, 2022.
[50] P. Bowlan, E. Martinez-Moreno, K. Reimann, M. Woerner, and T. Elsaesser, "Terahertz radiative coupling and damping in multilayer graphene," *New J. Phys.*, vol. 16, no. 1, 2014, Art. no. 013027.
[51] C. H. Costa, L. F. Pereira, and C. G. Bezerra, "Light propagation in quasiperiodic dielectric multilayers separated by graphene," *Phys. Rev. B*, vol. 96, no. 12, 2017, Art. no. 125412.
[52] Q. Gong and X. Hu, *Photonic Crystals: Principles and Applications*. Boca Raton, FL, USA: CRC press, 2014.
[53] B.-Z. Xu, C.-Q. Gu, Z. Li, and Z.-Y. Niu, "A novel structure for tunable terahertz absorber based on graphene," *Opt. Exp.*, vol. 21, no. 20, pp. 23803–23811, 2013.
[54] A. Andryieuski and A. V. Lavrinenko, "Graphene metamaterials based tunable terahertz absorber: Effective surface conductivity approach," *Opt. Exp.*, vol. 21, no. 7, pp. 9144–9155, 2013.
[55] T. Wang, Y. Zhang, H. Zhang, and M. Cao, "Dual-controlled switchable broadband terahertz absorber based on a graphene-vanadium dioxide metamaterial," *Opt. Mater. Exp.*, vol. 10, no. 2, pp. 369–386, 2020.
[56] R. Cheng *et al.*, "Tunable graphene-based terahertz absorber via an external magnetic field," *Opt. Mater. Exp.*, vol. 10, no. 2, pp. 501–512, 2020.
[57] K. Meng *et al.*, "Tunable broadband terahertz polarizer using graphene-metal hybrid metasurface," *Opt. Exp.*, vol. 27, no. 23, pp. 33768–33778, 2019.
[58] Q. Bao *et al.*, "Broadband graphene polarizer," *Nature Photon.*, vol. 5, no. 7, pp. 411–415, 2011.
[59] C. Pei *et al.*, "Broadband graphene/glass hybrid waveguide polarizer," *IEEE Photon. Technol. Lett.*, vol. 27, no. 9, pp. 927–930, May 2015.
[60] F. A. Juneghani, A. Zeidaabadi-Nezhad, and R. Safian, "Analysis of diffraction graphene gratings using the C-method and design of a terahertz polarizer," *Prog. Electromagnetics Res. M*, vol. 65, pp. 175–186, 2018.
[61] W. Lai, H. Yuan, H. Fang, Y. Zhu, and H. Wu, "Ultrathin, highly flexible and optically transparent terahertz polarizer based on transparent conducting oxide," *J. Phys. D: Appl. Phys.*, vol. 53, no. 12, 2020, Art. no. 125109.
[62] D. Sarker, P. P. Nakti, M. I. Tahmid, M. A. Z. Mamun, and A. Zubair, "Terahertz polarizer based on tunable surface plasmon in graphene nanoribbon," *Opt. Exp.*, vol. 29, no. 26, pp. 42713–42725, Dec. 2021.